### Title

Preordering of water is not needed for ice recognition by hyperactive antifreeze proteins




### Journal

Proceedings of the National Academy of Sciences of the United States of America, 115(33)

### ISSN

0027-8424



### Authors

Hudait, Arpa
Moberg, Daniel R
Qiu, Yuqing
et al.



### Publication Date

2018-08-14

### DOI

10.1073/pnas.1806996115

Peer reviewed

# Preordering of water is not needed for ice recognition by hyperactive antifreeze proteins

Arpa Hudait[a], Daniel R. Moberg[b], Yuqing Qiu[a], Nathan Odendahl[a], Francesco Paesani[b,1], and Valeria Molinero[a,1]

[a]Department of Chemistry, The University of Utah, Salt Lake City, UT 84112-0850; and [b]Department of Chemistry and Biochemistry, University of California, San Diego, La Jolla, CA 92093-0314

Edited by Pablo G. Debenedetti, Princeton University, Princeton, NJ, and approved June 15, 2018 (received for review April 23, 2018)

**Antifreeze proteins (AFPs) inhibit ice growth in organisms living in cold environments. Hyperactive insect AFPs are particularly effective, binding ice through "anchored clathrate" motifs. It has been hypothesized that the binding of hyperactive AFPs to ice is facilitated by preordering of water at the ice-binding site (IBS) of the protein in solution. The antifreeze protein *Tm*AFP displays the best matching of its binding site to ice, making it the optimal candidate to develop ice-like order in solution. Here we use multiresolution simulations to unravel the mechanism by which *Tm*AFP recognizes and binds ice. We find that water at the IBS of the antifreeze protein in solution does not acquire ice-like or anchored clathrate-like order. Ice recognition occurs by slow diffusion of the protein to achieve the proper orientation with respect to the ice surface, followed by fast collective organization of the hydration water at the IBS to form an anchored clathrate motif that latches the protein to the ice surface. The simulations suggest that anchored clathrate order could develop on the large ice-binding surfaces of aggregates of ice-nucleating proteins (INP). We compute the infrared and Raman spectra of water in the anchored clathrate motif. The signatures of the OH stretch of water in the anchored clathrate motif can be distinguished from those of bulk liquid in the Raman spectra, but not in the infrared spectra. We thus suggest that Raman spectroscopy may be used to probe the anchored clathrate order at the ice-binding surface of INP aggregates.**

antifreeze protein | molecular recognition | interfacial water | vibrational spectroscopy | ice

Several organisms have evolved antifreeze proteins (AFPs) that recognize and bind ice (1–3). The recognition of ice by proteins in solution has been considered the most challenging recognition problem in biology (4). The key question is, how do AFPs distinguish between different phases of water, liquid, and ice to recognize and bind the latter? While crystallographic data provide important insights on the binding of AFPs to ice (5–7), it is not yet possible to resolve the microscopic process of ice recognition and binding with state-of-the-art experimental methods. In a pioneering simulation study of the hyperactive AFP of *Spruce budworm* (*Cf*AFP) in solution, Nutt and Smith reported a small enhancement of the local tetrahedral order of water at 2.3 Å from the ice-binding site (IBS) (8). Building on that result, they hypothesized that interfacial water hydrating the IBS of the hyperactive protein could form an ice-like layer in solution that would facilitate ice recognition and a seamless integration of the AFP to the ice/water interface (8). This conjecture has been widely accepted in the literature (3). Recent studies, however, demonstrate that preordering of interfacial water is not a requisite for ice recognition: polyvinyl alcohol is a flexible polymer that strongly binds to ice, yet it does not induce ice-like order in the liquid (9). The "preordering-binding" hypothesis has never been tested for ice-binding proteins.

The IBS of hyperactive insect AFPs is flat and consists of a regular array of threonine residues, TxT (where T is threonine and x a nonconserved amino acid) that creates a 2D lattice-like arrangement with distances between the hydroxyl groups of the threonine residues comparable to those between the water molecules at the prismatic and basal planes of ice (Fig. 1*A*). Hyperactive AFPs bind to both the prismatic and basal plane of ice through "anchored clathrate" (AC) motifs (5, 10), in which a clathrate-like arrangement around the methyl groups of the threonine residues is anchored to the protein via the hydroxyl groups of the same amino acids (Fig. 1*B*). The AFP of *Tenebrio molitor*, *Tm*AFP, has the best matching to ice among hyperactive AFPs, making it the ideal candidate for the development of ice-like or AC-like order at the IBS in solution (10).

NMR and molecular simulations indicate that the water molecules in the channel between the two rows of threonine residues in the IBS of *Tm*AFP exchange with the bulk liquid in subnanosecond time scales (10, 11). It is difficult to reconcile this relatively fast exchange with ice-like order at the IBS. Moreover, a recent vibrational sum-frequency generation spectroscopic study of the hydration water of the IBS of *D*AFP-1, a structural homolog of *Tm*AFP, at the water/vapor interface did not find ice-like order (12). In that study, however, the protein accumulated at the water/vapor interface with the IBS of the protein oriented toward the vapor phase, which may result in dewetting of the binding surface. Therefore, the solvation of the IBS at the water/vapor interface may not be representative of the hydration of the protein immersed in liquid water. To date, the mechanism by which hyperactive AFPs bind to ice, the order of water at the IBS in solution, and the spectroscopic signatures of water in solution and ice-bound states, are not known.

Here we use multiresolution molecular dynamics simulations to elucidate how *Tm*AFP recognizes and binds ice, and to determine if water ordering at the binding site is involved in the

## Significance

**Antifreeze proteins have evolved to inhibit ice growth in organisms living at subfreezing temperatures; the mechanism by which these proteins recognize and bind ice is not understood. It has been proposed that antifreeze proteins recognize ice by preordering water at the ice-binding site already in solution. Here we use multiresolution molecular simulations to demonstrate that preordering of interfacial water is not needed for ice recognition by antifreeze proteins. We predict that preordering could emerge on the large ice-binding surfaces of aggregates of ice-nucleating proteins, where it may assist with ice nucleation.**

Author contributions: A.H., F.P., and V.M. designed research; A.H. and D.R.M. performed research; A.H., D.R.M., Y.Q., N.O., F.P., and V.M. analyzed data; and A.H., D.R.M., F.P., and V.M. wrote the paper.

The authors declare no conflict of interest.

This article is a PNAS Direct Submission.



See Commentary on page 8244.

[1]To whom correspondence may be addressed. Email: fpaesani@ucsd.edu or valeria.molinero@utah.edu.

This article contains supporting information online at www.pnas.org/lookup/suppl/doi:10.1073/pnas.1806996115/-/DCSupplemental.

Published online July 9, 2018.

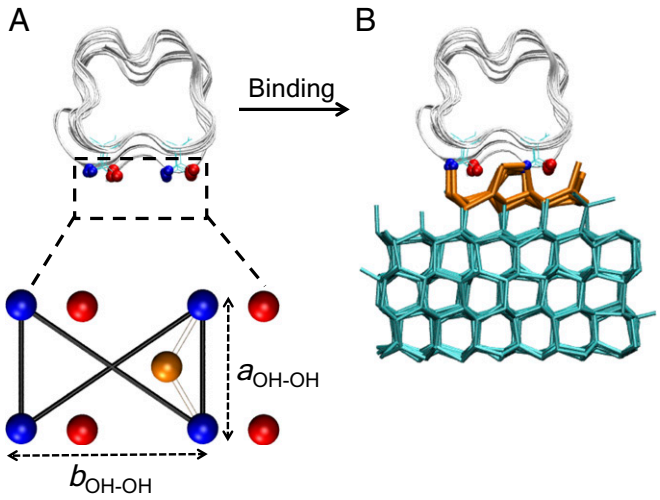


**Fig. 1.** Structure of *Tm*AFP and its binding to ice. (*A*) Side view of *Tm*AFP. The threonine residues at the IBS are shown inside the dotted region. The hydroxyl and methyl groups of the threonine at the IBS are shown with blue and red balls, respectively. The protein backbone is shown with a silver ribbon. The distances $a_{OH\text{-}OH}$ and $b_{OH\text{-}OH}$ between the hydroxyl groups at the IBS are used to compute the lattice mismatch ($\delta a$, $\delta b$) between hydroxyl groups at the ice-binding surface and ice: $\delta a = [(a_{OH\text{-}OH} - a_{ice})/a_{ice}] \times 100\%$, and $\delta b = [(b_{OH\text{-}OH} - b_{ice})/b_{ice}] \times 100\%$, where $a_{ice}$ and $b_{ice}$ are the ice lattice parameters at the ice surface. The average lattice mismatch of *Tm*AFP to the basal plane of ice, $\delta a = 7.2\%$ and $\delta b = -6.7\%$, is the lowest among hyperactive insect AFPs. The orange ball shows a channel water occupying the trough between two rows of threonine residues (10). (*B*) Snapshot of *Tm*AFP bound to the basal plane of ice. The AC motif that binds *Tm*AFP to ice is shown with orange sticks (10), the ice with cyan sticks, and liquid water is not shown, for clarity.

process of ice recognition. Through a combination of simulations with fully atomistic and united atom models, we determine the structure, infrared, and Raman spectra of the interfacial water in the OH-stretch region, and the molecular mechanism of ice recognition and binding.

## IBS of the AFP Does Not Induce Ice-Like Order in Solution

We model water with three levels of resolution: the fully flexible atomistic polarizable many-body MB-pol model (13–15), the rigid atomistic nonpolarizable TIP4P/2005 model (16), and the coarse-grained many-body mW model (17). *Tm*AFP is modeled with the fully atomistic flexible CHARMM22 force field with CMAP correction (18) when combined with the TIP4P/2005 and MB-pol water models. *Tm*AFP in the simulations with mW water is modeled as a rigid body at the united atom level (i.e., no hydrogen atoms) with parameters that reproduce the solvation structure around the protein and the structure of the AC motif (Fig. 1*B*) of the atomistic model (10).

We investigate the structure of water around *Tm*AFP in solution through metrics designed to quantify tetrahedral order and to identify ice and the AC motif. The tetrahedral order of the first shell of water in contact with the ice-binding surface of *Tm*AFP, measured through $S_g$ (19) or $q_{tet}$ (20), is significantly lower than for ice or the AC, and slightly diminished with respect to bulk water for both the mW and TIP4P/2005 models (*SI Appendix*, Figs. S2 and S3). These results are in agreement with prior simulation studies for *Tm*AFP and *Cf*AFP using the TIP4P (21), TIP4P/2005 (22), and TIP5P (8) models. We find the bond order parameter $q_3$ (23) of water at the IBS, which also provides a measure of ordering, to be slightly larger than in bulk liquid but significantly smaller than in the AC or ice (Fig. 2). We note that the degree of ordering is identical for the MB-pol, TIP4P/2005 and mW models (Fig. 2). We conclude that water at the IBS of *Tm*AFP in solution does not display ice-like or AC-like order.

Bacterial ice-nucleating proteins (INPs) share with *Tm*AFP the presence of TxT repeats in their ice-binding surfaces. The repeats in the INPs, however, are much longer than in AFPs (25, 26). The monomer of the INP of *Pseudomonas syringae*, *Ps*INP, has 67 loops that contain the TxT sequence and nucleates ice with modest efficiency, at −26 °C (27). Aggregates of this protein in the cell membrane, however, can nucleate ice at temperatures as high as −2 °C (25). Fig. 3 shows the evolution of the ordering of interfacial water at 273 K as a function of the area of the IBS. Square-like TCT surfaces modeled as rigid bodies (red filled circles) order water more prominently than those in which the groups at the IBS fluctuate with the same magnitude as in the fully flexible atomistic *Tm*AFP model in solution (red empty circles) (10), consistent with previous results on the role of flexibility in water ordering at ice-nucleating alcohol monolayers (28). We note that the experimental flexibility of membrane-bound INPs is not yet known. Since assemblies of large bacterial INPs are anchored to the cell membrane, we expect that these protein aggregates experience far less conformational fluctuations than small AFPs in solution. Preordering of liquid water at the IBS of *P. syringae*, which is predicted to form multimeric aggregates with ∼50 *Ps*INP monomers in the cell wall (29–32), will be pronounced only if the protein aggregates exhibit structural rigidity. Experimental characterization of the conformational fluctuations of membrane-bound protein assemblies is therefore necessary to accurately predict the degree of water ordering induced by bacterial INPs.

We find that the extent of water ordering on rigid peptide surfaces is quite insensitive to the length of surfaces that have a single row of TCT (rectangular surfaces, cyan line in Fig. 3). However, aggregation of the TCT peptides to produce square-like IBS results in a steady increase of water ordering with area (solid red line in Fig. 3). To understand this difference, we note that interfaces typically impact water ordering over length scales of ∼1 nm (33–36), which is the width of the rectangular peptide surfaces. We indeed find that the ordering of water over the outermost rows of threonine on the square-like peptide surfaces is lower than in the middle region and comparable to that on the rectangular TCT surfaces (*SI Appendix*,

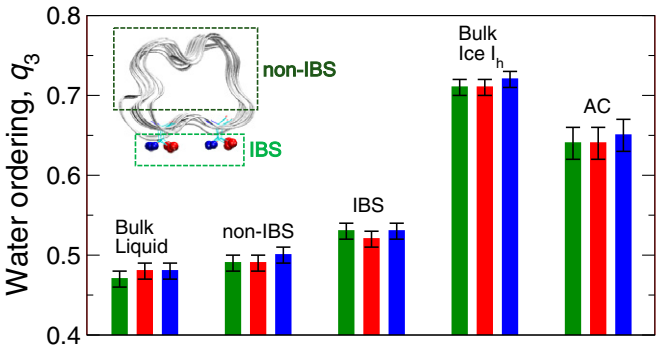


**Fig. 2.** Comparison of the order of interfacial water of *Tm*AFP in solution, bound to ice, and of pure water in the bulk liquid and hexagonal ice phases. Water ordering for different planes of protein for different models of water: TIP4P/2005 (red), MB-pol (blue), and mW (green). The averaged $q_3$ values are computed at 273 K for mW water and at 252 K for TIP4P/2005 and MB-pol water models. These temperatures correspond to the melting temperatures of mW and TIP4P/2005, respectively (16, 17, 24). The $q_3$ value for the AC motif is computed for *Tm*AFP bound to the basal plane of ice. For all the water models, the ordering of water at the IBS is nominally higher than in bulk but far away from that of the ice $I_h$ and AC motif. The tetrahedral order at the binding site, however, is lower than in bulk liquid water (*SI Appendix*, Figs. S2 and S3). (*Inset*) Sketches of the regions where water molecules are considered to be part of IBS and non-IBS; a more detailed drawing of these regions is shown in *SI Appendix*, Fig. S1.

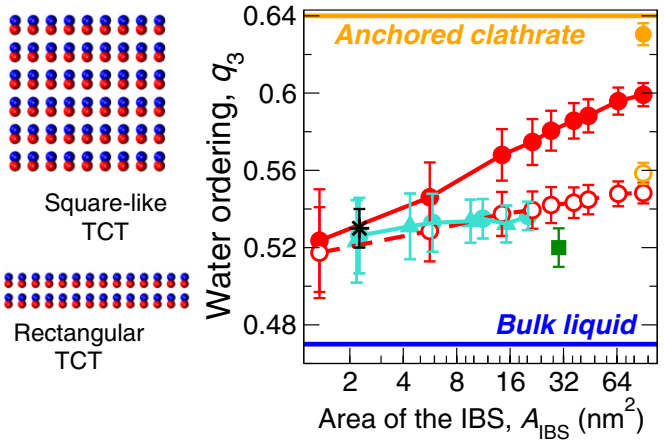


**Fig. 3.** Ordering of interfacial water by peptide surfaces as a function of the area of the ice-binding surface. (*Left*) Square and rectangular TCT surfaces expose pairs of rows of threonine residues (methyl in red, hydroxyl in blue) to water. (*Right*) Ordering of interfacial water. The red circles show the average $q_3$ value for water at the IBS of square-like surfaces that repeat the TCT amino acid sequence: red filled circles correspond to rigid surfaces and red empty circles to surfaces in which the IBS has the same flexibility as the fully flexible atomistic *Tm*AFP model in TIP4P/2005 water (*SI Appendix, Supporting Methods S3.2.4*). The degree of water ordering significantly diminishes when flexibility is introduced to the hydroxyl and methyl groups at the IBS. The cyan symbols show the averaged $q_3$ for water at the IBS of rigid rectangular TCT surfaces (cyan circles) and *Tm*AFP-like proteins built by repeating a single loop of *Tm*AFP (cyan triangles). A rigid monomer of *Ps*INP with 67 TxT repeats with same lattice mismatch as *Tm*AFP (10) exhibits nearly the same degree of water ordering at the IBS (green square) as *Tm*AFP. The TCT surfaces have the same average lattice mismatch as that of *Tm*AFP, $\delta a$ = 7.2% and $\delta b$ = −6.7%. The proteins that repeat a single loop of *Tm*AFP have a lattice mismatch to ice, $\delta a$ = 7.2% and $\delta b$ = −9.3%. All peptide surfaces are modeled at the united atom level and solvated with mW water, except for *Tm*AFP (black star) that is modeled at the united atom and fully atomistic levels producing the same water ordering (Fig. 2). The degree of water ordering gradually increases with the area of the IBS for rigid square-like TCT surfaces, approaching the $q_3$ of the AC motif of the bound protein (orange line). A rigid periodic TCT surface with the same mismatch to ice as *Tm*AFP acquires AC order in solution (filled orange circle), in agreement with the results of ref. 54. Flexibility of the IBS decreases the order of the periodic TCT surface (empty orange circle). Hyperactive insect AFPs *Cf*AFP (55) and *Ri*AFP (56) have $A_{IBS}$ 2.7 and 4.2 nm$^2$, respectively, and poorer lattice mismatch to ice compared with *Tm*AFP (10). We expect the degree of water ordering at the IBS of *Cf*AFP and *Ri*AFP to be similar to the one for *Tm*AFP.

Fig. S4). It is important to note, however, that even rectangular surfaces that do not induce significant ordering of interfacial water, e.g., the monomer of *Ps*INP, can nucleate ice (10).

## AC Cannot Be Distinguished from Protein Hydration Water Through OH-Stretch Infrared or Raman Spectroscopy

Since the frequencies of the OH-stretching vibrations of the water molecules are extremely sensitive to the surrounding environment, vibrational spectroscopy represents a powerful tool to investigate the structure and dynamics of water in different phases, from bulk liquid water and ice to aqueous interfaces (37–39). Vibrational sum-frequency generation spectra of the OH-stretch region of water at the IBS of *D*AFP-1, a homolog of *Tm*AFP, did not reveal signatures of ice-like ordering (12). In that experiment the protein was studied at the water/vapor interface, where it accumulated with the amphiphilic IBS oriented toward the vapor phase (12), consistent with the hydration free energies computed in ref. 40. Our atomistic simulations indicate that the IBS of *Tm*AFP at the liquid/vapor interface is partially dewetted, retaining only the channel water (*SI Appendix*, Fig. S5). This indicates that to elucidate the structure of water at the IBS, the protein must be studied in solution.

Here we investigate whether it is possible to distinguish the signatures of the AC motif that binds *Tm*AFP to ice through OH-stretch infrared or Raman spectroscopies. Fig. 4 present the infrared and (unpolarized) Raman spectra of hydration water at the IBS and non-IBS of *Tm*AFP, the AC motif, ice, and liquid in the OH-stretch region computed with the MB-pol water model. The OH stretch of the hydration water at the IBS and non-IBS of *Tm*AFP are nearly indistinguishable in both the IR and Raman spectra (Fig. 4), consistent with the lack of ice-like or AC-like order at the IBS in solution. The IR spectra of the AC cannot be resolved from that of liquid water; both are broader and more blue-shifted than the spectrum of ice $I_h$. These results suggest that infrared spectroscopy will be unable to resolve the binding of AFPs to ice.

The AC is clearly distinguishable from bulk liquid in the Raman spectra, showing traces of the stronger frequency of ice $I_h$ at 3430 cm$^{-1}$, which can be attributed to antisymmetric stretching modes (41, 42), or—more accurately—to modes displaying strong intermolecular interactions (43–45), albeit with the characteristic broad lineshape of liquid water. However, both the infrared and Raman spectra of the AC motif are still strongly overlapped with the spectra of the protein solvation shell in solution. This suggests that it would also be challenging to establish whether the AFP is ice-bound or in solution from Raman spectroscopy.

## Molecular Mechanism of Ice Recognition and Binding

The lack of ice or AC order around *Tm*AFP in solution indicates that the IBS must build the AC order concurrent with its binding to the ice surface. Atomistic and united atom simulations that start with *Tm*AFP in solution show that the protein tumbles as it approaches the ice surface, until it finds the orientation and distance that allows the formation of the AC motif (Fig. 5*A*). After the protein aligns with its IBS parallel to both the ice surface and one of the three degenerate *a* axes ($a_1$, $a_2$, or $a_3$) of the basal plane, the water molecules between the protein and ice order into the AC motif within a few nanoseconds in atomistic simulations and within ∼0.1 ns in the united atom model [the ratio of these two time scales is consistent with the ratio of the diffusion coefficients in the respective water models at the corresponding temperatures, $D_{mW}$(273 K)/$D_{TIP4P/2005}$(246 K) ∼ 16] (17, 46). We conclude that the binding of *Tm*AFP to ice is a cooperative, all-or-nothing mechanism in which the 10 threonine residues bind simultaneously to ice.

Achieving protein orientations conducive to recognition and binding of the ice surface is a slow and diffusive process. To determine at which stage of the approach of the protein to the ice/water interface the AC motif is formed, we investigate the process of binding with the center of mass of *Tm*AFP restrained at a distance of ∼14.5 Å from the ice surface. At this distance the surface of ice needs to grow two bilayers (∼7.1 Å) to bind to the IBS of the protein. We find that *Tm*AFP binds to ice only when the IBS is aligned to one of the *a* axes of the basal plane ($\theta \sim 0°, 60°, 120°$) and the plane of the IBS is parallel to the plane of ice ($\phi \sim 0°$) (Fig. 5 *B* and *C* and *SI Appendix*, Figs. S8 and S9). We note that the binding and unbinding of the protein in Fig. 5 *B* and *C* and *SI Appendix*, Fig. S8 is a result of the distance restraint between the center of mass of the protein and the ice surface, which strains the ice-binding motif. The binding of *Tm*AFP to ice is irreversible in unconstrained simulations (10) and experiments (47). Our results indicate that preordering of interfacial water at the IBS of hyperactive AFPs is not a requisite for ice recognition and binding. Instead, ice recognition occurs by collective reorganization of the water between ice and the IBS, after the protein achieves the required orientation for binding to ice.

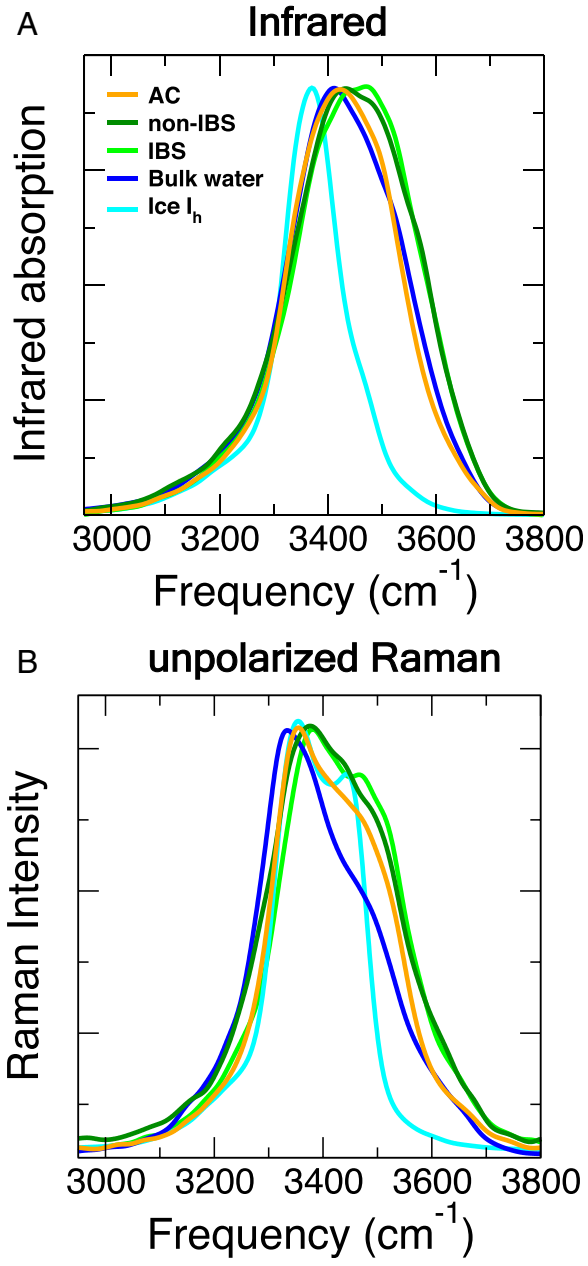


**Fig. 4.** Calculated infrared and Raman spectra of the interfacial water of *Tm*AFP. (*A*) Infrared and (*B*) unpolarized Raman spectra of OH-stretching frequency for bulk ice (cyan), bulk water (blue), water solvating the IBS (light-green line), and non-IBS (dark green) of *Tm*AFP in solution, and the AC motif that binds *Tm*AFP to the basal plane of ice (orange). The intensity of each spectrum is shown normalized by its maximum. The spectra reported here are computed with the 1B + 2B + NB approximation to the dipole moment surface from classical MD simulations evolved with MB-pol, starting from configurations equilibrated with TIP4P/2005. Spectra of ice $I_h$ is computed at 248 K, bulk water at 250 K, solvation water in the liquid at 252 K, and AC at 246 K. The spectrum of the ice bilayer (*SI Appendix*, Fig. S6) below the AC binding motif indicates that the AC structure seamlessly integrates to ice. *SI Appendix*, Fig. S7 shows the infrared and Raman spectra of the AC with error bars. All spectra have been red-shifted by 168–171 $cm^{-1}$ for simulations at 246 to 252 K, respectively, to account for nuclear quantum effects as follows from de Broglie's relationship (45, 49, 57).

## Conclusions and Outlook

In this study, we use molecular simulations with three levels of resolution to elucidate the mechanism by which *Tm*AFP recognizes ice, and the spectroscopic signatures of the AC motif that binds the protein to ice. We find that water at the ice-binding surface of hyperactive AFPs does not have ice-like or AC-like order in solution. Instead, ice recognition is achieved by slow diffusion of the protein to find the proper orientation with respect to the ice surface, followed by fast collective organization of the hydration water at the IBS of *Tm*AFP to form the AC motif that seals the protein to the crystal surface. We conclude that preordering of interfacial water at the IBS is not required for ice recognition by hyperactive AFPs.

The most potent synthetic ice recrystallization inhibition molecule, polyvinyl alcohol (PVA), has been recently shown to bind ice through a cooperative zipper mechanism (9). The cooperativity is found to arise from a different scaling in the loss of entropy and gain of enthalpy upon binding of each monomer: Binding of the first monomer results in loss of the center-of-mass translational entropy, while binding of subsequent monomers results in progressively smaller losses of configurational entropy of the polymer chain (9). As *Tm*AFP is conformationally rigid (12, 48), the entropy loss upon binding is even smaller than for

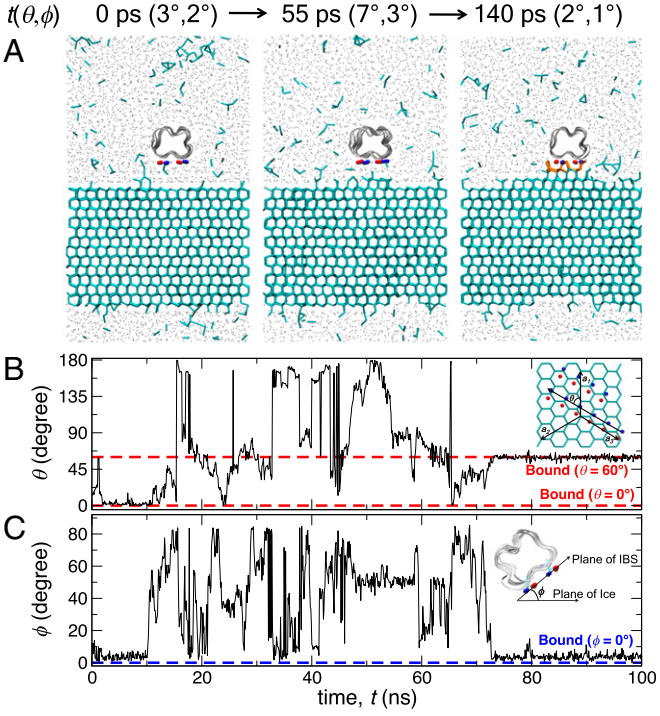


**Fig. 5.** Molecular mechanism of ice recognition by *Tm*AFP. (*A*) Snapshots of a typical binding event of *Tm*AFP to the basal plane ice in a united atom simulation. The color scheme is the same as in Fig. 1. The cyan sticks show all water molecules that are identified as ice (considering cubic and hexagonal ice) using the CHILL+ algorithm (58). Water molecules in the liquid are shown with gray points and the AC motif with orange sticks. (*B*) Time evolution of the orientation $\theta$ of the main axis of *Tm*AFP with respect to the $a_1$ axis of the basal ice surface (see sketch in inset) along a 100-ns simulation of *Tm*AFP with its center of mass restrained to ~14.5 Å from the ice surface. (*C*) Time evolution of the tilt $\phi$ of the main axis of *Tm*AFP with respect to the plane of the surface (see sketch in the *Inset)* along the same simulation as in *B*. We expect that binding of the protein to the primary prismatic plane of ice occurs only when the protein is aligned in the *c* II or *c* ⊥ orientations and the plane of the IBS is parallel to the plane of ice (10). The time evolutions of $\phi$ and $\theta$ are qualitatively similar in all restrained simulations of protein binding (*SI Appendix*, Fig. 8). A free-energy landscape $G(\theta,\phi)$ built from 15 independent simulations of binding of restrained *Tm*AFP, each 100 ns long, is shown in *SI Appendix*, Fig. S9 and supports the existence of three distinct bound states on the basal plane, with the long axis of the protein aligned with each of the three *a* axes of the crystal.

PVA, which explains its stronger binding to ice (9, 10). We conjecture that evolution has favored rigid IBS for hyperactive AFPs and INPs because it results in stronger binding to ice, which for INPs leads to higher ice-nucleation efficiency (28).

This study directly probes infrared and Raman spectroscopic signatures in the OH-stretch region of the AC motif. Our results indicate that the AC could be distinguished from bulk liquid in Raman, but not in the infrared spectra. Identification of the AC with vibrational spectroscopy would still be challenging, as both the infrared and Raman spectra of the AC motif overlap with that of water hydrating the IBS of *Tm*AFP. We suggest that Raman, as well as other advanced vibrational spectroscopic techniques, could be used to probe the structure of water at the ice-binding surface of extended aggregates of INPs, which may achieve AC-like ordering already in solution.

## Materials and Methods

**Model and Simulation Details.** The all-atom model of *Tm*AFP is built from its crystal structure in the Protein Data Bank (PDB ID code 1EZG), using CHARMM22 force field with CMAP correction (18) as in ref. 10. Water is modeled at the rigid nonpolarizable atomistic level with the TIP4P/2005 model (16). The infrared and unpolarized Raman spectra of water are computed from many-body molecular dynamics (MB-MD) simulations in which the interactions between water molecules are computed with the MB-pol potential (13–15, 49), which has been shown to exhibit chemical and spectroscopic accuracy (50). The intraprotein and water–protein interactions are modeled with the same parameters as that in atomistic simulations performed with the CHARMM22 force field for protein and TIP4P/2005 model for water. Water in the united atom simulations is modeled with the monoatomic water model mW (17), which reproduces the structure and thermodynamics of liquid water and ice at a fraction of the computational cost compared with the atomistic water models (51). The united atom model of *Tm*AFP is built from the crystal structure 1EZG (Protein Data Bank ID), and modeled as a rigid body. Each heavy atom of the protein interacts with mW water through a Stillinger–Weber potential (52) with the parameters of ref. 10. The same united atom protein–water interaction parameters of *Tm*AFP are used to model the INP *Ps*INP (10), TCT peptide surfaces, and *Tm*AFP-like proteins. To model the flexible TCT peptide surfaces, intramolecular flexibility is added to the threonine residues at the IBS through a harmonic restraint that lets the methyl and hydroxyl groups vibrate around their initial positions. The force constant of the harmonic spring, $k = 8$ kcal mol$^{-1}$ Å$^{-2}$, reproduces the intramolecular flexibility of the fully flexible atomistic *Tm*AFP in TIP4P/2005 water (10).

**Calculations of Infrared and Raman Spectra.** The infrared spectra are calculated from the dipole moment surface (49). To generate the system dipole moment, the 1B + 2B + NB MB-$\mu$ dipole moment surface treatment is used, combining explicit 1-body and 2-body terms with inductive contributions from higher *N*-body terms (49). Similarly for the (unpolarized) Raman spectra, the 1B + 2B + NB MB-$\alpha$ approximation to the polarizability tensor is used to calculate the system polarizability tensors. The system dipole moments and system polarizability tensors are then used to calculate the appropriate time-correlation functions from which the desired spectra are obtained. The details of the water molecules included in the dipole moment and polarizability tensor calculations are given in *SI Appendix, Supporting Methods S1.4*.

**Constrained Simulations of *Tm*AFP Binding to Ice.** To perform the constrained simulations of binding of united atom *Tm*AFP to mW ice we use a simulation cell of ice/water coexistence containing an ice slab with six bilayers in contact with liquid water on one side and vapor on the other side. The positions of the water molecules in the two bilayers in contact with vacuum are fixed (equations of motion not integrated). In these simulations we control two variables at the same time: (*i*) the distance between the center of mass of the protein and ice/water interface, and (*ii*) the amount of ice and liquid. We control the distance between the center of mass of the protein and ice/water interface with a harmonic spring, with force constant of 50 kcal mol$^{-1}$ Å$^{-2}$. The harmonic spring is allowed to fluctuate only in the direction orthogonal to the ice/water interface. The amount of ice and liquid is controlled by constraining the global value of the bond order parameter $Q_6$ (10, 53), where the equilibrium value of $Q_6$ is determined from the initial configuration of the two-phase system. The restraint to maintain the amount of ice is applied to all of the mobile water molecules, i.e., all except those in the two fixed ice bilayers. The magnitude of the restrain to maintain the amount of ice is determined from the force constant equal to 20 kcal mol$^{-1}$ multiplied by the number of mobile water molecules.

**ACKNOWLEDGMENTS.** We thank Christopher Knight for providing a simulation cell for the atomistic ice model, and Heather C. Allen and Justin J. Talbot for valuable suggestions and discussions. This work was supported by the National Science Foundation through Award CHE-1305427 "Center for Aerosols Impacts on Climate and the Environment." We thank the Center for High Performance Computing at The University of Utah for technical support and a grant of computer time.

1. Bar Dolev M, Braslavsky I, Davies PL (2016) Ice-binding proteins and their function. *Annu Rev Biochem* 85:515–542.
2. Yeh Y, Feeney RE (1996) Antifreeze proteins: Structures and mechanisms of function. *Chem Rev* 96:601–618.
3. Davies PL (2014) Ice-binding proteins: A remarkable diversity of structures for stopping and starting ice growth. *Trends Biochem Sci* 39:548–555.
4. Sharp KA (2011) A peek at ice binding by antifreeze proteins. *Proc Natl Acad Sci USA* 108:7281–7282.
5. Garnham CP, Campbell RL, Davies PL (2011) Anchored clathrate waters bind antifreeze proteins to ice. *Proc Natl Acad Sci USA* 108:7363–7367.
6. Leinala EK, et al. (2002) A β-helical antifreeze protein isoform with increased activity. Structural and functional insights. *J Biol Chem* 277:33349–33352.
7. Liou Y-C, Tocilj A, Davies PL, Jia Z (2000) Mimicry of ice structure by surface hydroxyls and water of a beta-helix antifreeze protein. *Nature* 406:322–324.
8. Nutt DR, Smith JC (2008) Dual function of the hydration layer around an antifreeze protein revealed by atomistic molecular dynamics simulations. *J Am Chem Soc* 130:13066–13073.
9. Naullage PM, Lupi L, Molinero V (2017) Molecular recognition of ice by fully flexible molecules. *J Phys Chem C* 121:26949–26957.
10. Hudait A, Odendahl N, Qiu Y, Paesani F, Molinero V (2018) Ice-nucleating and antifreeze proteins recognize ice through a diversity of anchored clathrate and ice-like motifs. *J Am Chem Soc* 140:4905–4912.
11. Modig K, Qvist J, Marshall CB, Davies PL, Halle B (2010) High water mobility on the ice-binding surface of a hyperactive antifreeze protein. *Phys Chem Chem Phys* 12:10189–10197.
12. Meister K, et al. (2015) Investigation of the ice-binding site of an insect antifreeze protein using sum-frequency generation spectroscopy. *J Phys Chem Lett* 6:1162–1167.
13. Babin V, Leforestier C, Paesani F (2013) Development of a "first principles" water potential with flexible monomers: Dimer potential energy surface, VRT spectrum, and second virial coefficient. *J Chem Theory Comput* 9:5395–5403.
14. Babin V, Medders GR, Paesani F (2014) Development of a "first principles" water potential with flexible monomers. II: Trimer potential energy surface, third virial coefficient, and small clusters. *J Chem Theory Comput* 10:1599–1607.
15. Medders GR, Babin V, Paesani F (2014) Development of a "first-principles" water potential with flexible monomers. III. Liquid phase properties. *J Chem Theory Comput* 10:2906–2910.
16. Abascal JLF, Vega C (2005) A general purpose model for the condensed phases of water: TIP4P/2005. *J Chem Phys* 123:234505.
17. Molinero V, Moore EB (2009) Water modeled as an intermediate element between carbon and silicon. *J Phys Chem B* 113:4008–4016.
18. MacKerell AD, et al. (1998) All-atom empirical potential for molecular modeling and dynamics studies of proteins. *J Phys Chem B* 102:3586–3616.
19. Chau PL, Hardwick AJ (1998) A new order parameter for tetrahedral configurations. *Mol Phys* 93:511–518.
20. Errington JR, Debenedetti PG (2001) Relationship between structural order and the anomalies of liquid water. *Nature* 409:318–321.
21. Midya US, Bandyopadhyay S (2014) Hydration behavior at the ice-binding surface of the Tenebrio molitor antifreeze protein. *J Phys Chem B* 118:4743–4752.
22. Duboué-Dijon E, Laage D (2014) Comparative study of hydration shell dynamics around a hyperactive antifreeze protein and around ubiquitin. *J Chem Phys* 141:22D529.
23. Steinhardt PJ, Nelson DR, Ronchetti M (1983) Bond-orientational order in liquids and glasses. *Phys Rev B Condens Matter* 28:784–805.
24. Reddy SK, et al. (2016) On the accuracy of the MB-pol many-body potential for water: Interaction energies, vibrational frequencies, and classical thermodynamic and dynamical properties from clusters to liquid water and ice. *J Chem Phys* 145:194504.
25. Maki LR, Galyan EL, Chang-Chien MM, Caldwell DR (1974) Ice nucleation induced by Pseudomonas syringae. *Appl Microbiol* 28:456–459.
26. Garnham CP, Campbell RL, Walker VK, Davies PL (2011) Novel dimeric β-helical model of an ice nucleation protein with bridged active sites. *BMC Struct Biol* 11:36.
27. Ling ML, et al. (2018) Effects of ice nucleation protein repeat number and oligomerization level on ice nucleation activity. *J Geophys Res Atmos* 123:1802–1810.
28. Qiu Y, et al. (2017) Ice nucleation efficiency of hydroxylated organic surfaces is controlled by their structural fluctuations and mismatch to ice. *J Am Chem Soc* 139:3052–3064.
29. Govindarajan AG, Lindow SE (1988) Size of bacterial ice-nucleation sites measured in situ by radiation inactivation analysis. *Proc Natl Acad Sci USA* 85:1334–1338.
30. Kajava AV, Lindow SE (1993) A model of the three-dimensional structure of ice nucleation proteins. *J Mol Biol* 232:709–717.
31. Burke MJ, Lindow SE (1990) Surface properties and size of the ice nucleation site in ice nucleation active bacteria: Theoretical considerations. *Cryobiology* 27:80–84.

32. Pandey R, et al. (2016) Ice-nucleating bacteria control the order and dynamics of interfacial water. *Sci Adv* 2:e1501630.
33. Xi E, et al. (2017) Hydrophobicity of proteins and nanostructured solutes is governed by topographical and chemical context. *Proc Natl Acad Sci USA* 114:13345–13350.
34. Patel AJ, Varilly P, Chandler D (2010) Fluctuations of water near extended hydrophobic and hydrophilic surfaces. *J Phys Chem B* 114:1632–1637.
35. Lee CY, McCammon JA, Rossky PJ (1984) The structure of liquid water at an extended hydrophobic surface. *J Chem Phys* 80:4448–4455.
36. Lee SH, Rossky PJ (1994) A comparison of the structure and dynamics of liquid water at hydrophobic and hydrophilic surfaces—A molecular dynamics simulation study. *J Chem Phys* 100:3334–3345.
37. Bakker HJ, Skinner JL (2010) Vibrational spectroscopy as a probe of structure and dynamics in liquid water. *Chem Rev* 110:1498–1517.
38. Björneholm O, et al. (2016) Water at interfaces. *Chem Rev* 116:7698–7726.
39. Perakis F, et al. (2016) Vibrational spectroscopy and dynamics of water. *Chem Rev* 116:7590–7607.
40. Schauperl M, et al. (2017) Balance between hydration enthalpy and entropy is important for ice binding surfaces in antifreeze proteins. *Sci Rep* 7:11901.
41. Whalley E (1977) A detailed assignment of the O–H stretching bands of ice I. *Can J Chem* 55:3429–3441.
42. Shigenari T, Abe K (2012) Vibrational modes of hydrogens in the proton ordered phase XI of ice: Raman spectra above 400 cm(−1). *J Chem Phys* 136:174504.
43. Sivakumar TC, Rice SA, Sceats MG (1978) Raman spectroscopic studies of the OH stretching region of low density amorphous solid water and of polycrystalline ice Ih. *J Chem Phys* 69:3468–3476.
44. Shi L, Gruenbaum SM, Skinner JL (2012) Interpretation of IR and Raman line shapes for H2O and D2O ice Ih. *J Phys Chem B* 116:13821–13830.
45. Moberg DR, Straight SC, Knight C, Paesani F (2017) Molecular origin of the vibrational structure of ice $I_h$. *J Phys Chem Lett* 8:2579–2583.
46. Rozmanov D, Kusalik PG (2012) Anisotropy in the crystal growth of hexagonal ice, I(h). *J Chem Phys* 137:094702.
47. Celik Y, et al. (2013) Microfluidic experiments reveal that antifreeze proteins bound to ice crystals suffice to prevent their growth. *Proc Natl Acad Sci USA* 110:1309–1314.
48. Daley ME, Sykes BD (2003) The role of side chain conformational flexibility in surface recognition by Tenebrio molitor antifreeze protein. *Protein Sci* 12:1323–1331.
49. Medders GR, Paesani F (2015) Infrared and Raman spectroscopy of liquid water through "first-principles" many-body molecular dynamics. *J Chem Theory Comput* 11:1145–1154.
50. Paesani F (2016) Getting the right answers for the right reasons: Toward predictive molecular simulations of water with many-body potential energy functions. *Acc Chem Res* 49:1844–1851.
51. Lu J, Qiu Y, Baron R, Molinero V (2014) Coarse-graining of TIP4P/2005, TIP4P-Ew, SPC/E, and TIP3P to monatomic anisotropic water models using relative entropy minimization. *J Chem Theory Comput* 10:4104–4120.
52. Stillinger FH, Weber TA (1985) Computer simulation of local order in condensed phases of silicon. *Phys Rev B Condens Matter* 31:5262–5271.
53. Lechner W, Dellago C (2008) Accurate determination of crystal structures based on averaged local bond order parameters. *J Chem Phys* 129:114707.
54. Midya US, Bandyopadhyay S (2017) Interfacial water arrangement in the ice-bound state of an antifreeze protein: A molecular dynamics simulation study. *Langmuir* 33:5499–5510.
55. Leinala EK, Davies PL, Jia Z (2002) Crystal structure of β-helical antifreeze protein points to a general ice binding model. *Structure* 10:619–627.
56. Hakim A, et al. (2013) Crystal structure of an insect antifreeze protein and its implications for ice binding. *J Biol Chem* 288:12295–12304.
57. Straight SC, Paesani F (2016) Exploring electrostatic effects on the hydrogen bond network of liquid water through many-body molecular dynamics. *J Phys Chem B* 120:8539–8546.
58. Nguyen AH, Molinero V (2015) Identification of clathrate hydrates, hexagonal ice, cubic ice, and liquid water in simulations: The CHILL+ algorithm. *J Phys Chem B* 119:9369–9376.